

## **KALMAN FILTER FOR REMOVAL OF SCALLOPING AND INTER-SCAN BANDING IN SCANSAR IMAGES**

**M. Iqbal, J. Chen<sup>\*</sup>, W. Yang, P. Wang, and B. Sun**

School of Electronics and Information Engineering, Beihang University, Beijing 100191, China

**Abstract**—Spaceborne synthetic aperture radar (SAR) plays more and more important role in Earth observation science, especially with ScanSAR mode which provides wide-swath coverage with moderate resolution. However, scalloping and inter-scan banding (ISB) are two major artifacts, which significantly degrade the quality of ScanSAR images. In this paper, a novel technique for removal of scalloping and ISB in ScanSAR images is proposed. Scalloping and ISB artifacts are modeled by two-dimensional gain and offset parameters varying as function of both azimuth time and range position. The gain and offset parameters can be split into azimuth and range components. The variations of gain/offset with respect to azimuth and range positions would represent scalloping and ISB artifacts respectively. In the proposed technique, recursive and minimum mean square error (MMSE) estimates of azimuth gain/offset parameters are found out by using Kalman filter for each azimuth location in a subswath by considering corresponding range samples as observation vector. Subsequently, range gain/offset parameters causing ISB artifacts are estimated by using Kalman filter for each range positions by considering azimuth samples as observation vector. The MMSE estimates of gain/offset parameters are used to directly remove scalloping and ISB artifacts. The proposed scheme was applied on simulated as well as calibrated real ScanSAR images. The experimental results exhibited the potential of proposed technique to be used as post processing tool for enhancing ScanSAR image quality.

---

*Received 21 August 2012, Accepted 27 September 2012, Scheduled 5 October 2012*

\* Corresponding author: Jie Chen (chenjie@buaa.edu.cn).

## 1. INTRODUCTION

Recent space missions had opened new horizons in the area of remote sensing. The spaceborne synthetic aperture radar (SAR) systems have attracted special interest in remote sensing tasks due to its high resolution [1,2], day/night operations, weather insensitivity and global coverage. Recently, SAR systems have been employed for environmental monitoring [3], surveillance [4,5], target identification [6], public security [7], navigation [8] and target recognition [9].

SAR systems are operated in various modes such as stripmap, ScanSAR, spotlight and etc.. In order to achieve wide swath in slant range, ScanSAR obtains multiple subswaths by tilting the antenna pattern in elevation. Due to scanning mechanism of ScanSAR, its system transfer function is time variant. The overall gain of system exhibits periodical variations over azimuth direction. The resulting periodic variations of output signal intensity as function of azimuth time is called scalloping.

TOPSAR (TOPS) [10] mode has demonstrated reduced scalloping compared to ScanSAR images, but it still requires scalloping correction processing. Moreover, TOPS achieves lower scalloping at the cost of sacrificing azimuth resolution. TOPS employs antenna electronically beam steering, and therefore, requires more T/R modules in radar antennas, leading to more expensive, higher weight, and difficult to be built. Also, not all SAR satellites can operate in TOPS mode, and therefore, employ ScanSAR mode to attain wide swathwidth SAR images. Hence scalloping removal is an important task in ScanSAR signal processing.

Several studies have been proposed to reduce scalloping effects in ScanSAR images. The first popular technique to remove scalloping was proposed by Bamler [11]. Bamler's technique involved computation of weighting factors to counter time variation of system function in azimuth direction. In his benchmark work, Vigneron [12] evaluated inverse antenna pattern and presented the state-of-the-art results that scalloping can be suppressed for high signal-to-noise ratio (SNR).

SAR systems can be calibrated by acquiring signals over areas having uniform backscatters. Shimada et al. [13,14] used Amazon forests for calibration of SAR systems by exploiting the fact that Amazon forests' backscatters are uniform and independent of incident angle. In [15], the authors extended their work to address scalloping artifacts using Amazon forests, and proposed an improved version of descalloping method of [11] by introducing a new normalization scheme that suppresses the deviation of power due to shift in estimated antenna

pattern. This method presented good calibration results in presence of slight deviation of antenna pattern.

Romeiser and et al. [16] proposed a descalloping filter based on post-processing modification of spectrum of ScanSAR image, in which the scalloping related peaks in the ScanSAR image spectrum are identified. The technique is iterated to refine filtering results. It results in lower SNR, and requires huge computational load due to processing of 50% overlapped sub-images and iterative nature of algorithms. An iterative mechanism was adopted by [17] to remove scalloping in ScanSAR images. They used the look-weighting method proposed by [11] along with iterative estimation of Doppler centroid. The technique proposed by [17] was not tested on real ScanSAR images though it worked well for simulated images.

The ScanSAR mode of operation suffers from another type of artifact which is called inter-scan banding (ISB). The ISB appears between two neighboring scans as intensity difference at the border of two scans. Even if range antenna pattern (RAP) is calculated exactly, ISB may occur due to temporal variation of RAP, noise floor and background intensities [15]. For Radarsat-1 and ENVISAT, ISB was corrected by updating roll angle and correcting range dependent gain by using overlap regions of two neighboring subswaths assuming RAPs are known [18]. A dynamic balancing method was proposed by [15] for removal of ISB by local intensity equalization.

In this paper, we propose a novel technique for removal of scalloping and inter-scan banding. We modeled scalloping by one-dimensional gain and offset parameters in [19], and employed Kalman filters to mitigate scalloping. In this paper, we extended our model to include ISB artifacts. In this paper, scalloping and ISB artifacts are modeled by two-dimensional gain and offset parameters varying as function of azimuth time and range positions. The variation of gain/offset as function of azimuth can represent periodic variations in azimuth and inter-swath random variations of phase (known as scalloping) whereas ISB can be represented by variation of gain/offset as function of range position. For sake of simplicity, gain/offset functions can be split into two independent one dimensional (1D) functions, varying in azimuth and range directions. The separability of gain and offset functions is justified due to existing independence between phenomena underlying scalloping and ISB artifacts. In the proposed technique, the recursive and minimum mean square error (MMSE) estimates of azimuth gain/offset parameters are found out for each azimuth location in an arbitrary subswath by using corresponding range samples as observation vector. These estimated gain/offset parameters are used to remove the scalloping artifact from ScanSAR

image. In the similar fashion, range gain/offset parameters are found out by using Kalman filter for each range position and ISB is removed with the help of the estimated parameters. The proposed scheme was tested on both simulated images and real ScanSAR images. The experimental results exhibit the potential of proposed framework to be applied as post processing tool in both calibrated and non-calibrated SAR images.

The rest of the paper is organized as follows. The overview of ScanSAR transfer function is given in Section 2. The proposed framework including ScanSAR image model is explained in Section 3 and simulation results are discussed in Section 4. Finally, the paper is concluded in Section 5.

## 2. SCANSAR TRANSFER FUNCTION

The ScanSAR operational diagram is shown in Fig. 1. Total swath width is divided into  $L$  number of subswaths and each subswath is covered by tilting antenna in elevation. The number of subswaths in case of Fig. 1 is four. Each subswath is illuminated for dwell time,  $T_D$  and it will return to the same swath number after time  $T_R$ . In the ScanSAR literature,  $T_R$  is called return time and it is less than SAR aperture time,  $T_F$ .

If we consider that  $S(\tau, t)$  is representation of SAR image in signal domain and  $S(r, x)$  is its corresponding representation in data domain

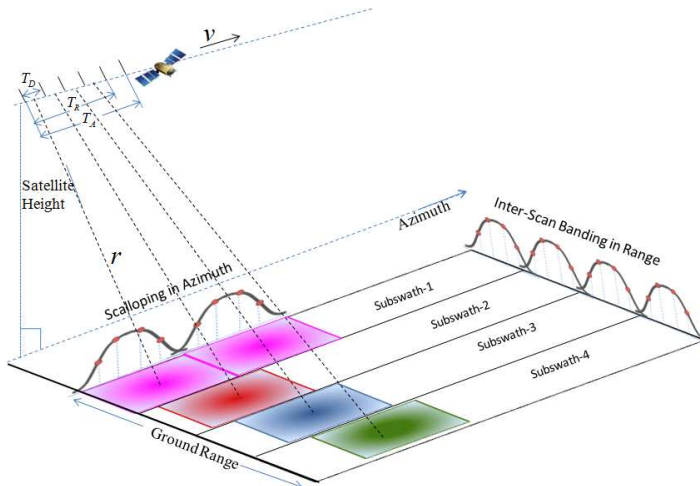


**Figure 1.** ScanSAR scheme.

where  $x$  is the closest approach time and  $r$  is the shortest slant range. The pulse response of a target located in  $(r, x)$  for SAR system can be given as [20]

$$h_{SAR}(\tau, t; r, x) = G_\varphi \left( \frac{v(t-x)}{r} \right) \delta \left( \tau - \frac{2\Delta R((t-x); r)}{c} \right) \exp \left( -j \left( \frac{4\pi}{\lambda} \Delta R((t-x); r) \right) \right) \quad (1)$$

where  $G_\varphi$  is azimuth antenna pattern (AAP) and it varies as a function of  $\varphi = vt/r$ .  $\delta(\tau)$  is the range compressed pulse delayed by antenna-target differential time with  $\Delta R$  defined as [20]

$$\Delta R(t-x; r) = R(t-x; r) - r \simeq \frac{v^2}{2r} (t-x)^2 \quad (2)$$

The third term in SAR pulse response given by (1) represents frequency dependent phase shift. Since pulse response of SAR depends on difference between current position of satellite and closest approach time so it is stationary in azimuth direction. ScanSAR is a special mode of operation of conventional SAR where sensor is operated into bursts over series of range subswaths as shown in Fig. 1. Thus pulse response of ScanSAR can be obtained from pulse response of SAR by windowing (1) with a square wave  $w_{SS}$  that implements mathematical model of ScanSAR operation shown in Fig. 1:

$$w_{SS}(\tau, t; r, x) = \sum_{k=-\infty}^{\infty} \text{rect} \left( \frac{t}{T_D} - kT_R \right) \quad (3)$$

The pulse response of ScanSAR can be given as [20]

$$h_{SS}(\tau, t; r, x) = G_\varphi \left( \frac{v(t-x)}{r} \right) f_r \otimes \sum_{k=-\infty}^{\infty} \text{rect} \left( \frac{t}{T_D} - kT_R \right) \quad (4)$$

where

$$f_r = \delta \left( \tau - \frac{2\Delta R((t-x); r)}{c} \right) \cdot \exp \left( -j \left( \frac{4\pi}{\lambda} \Delta R((t-x); r) \right) \right)$$

In (4),  $\otimes$  represent convolution. The pulse response of SAR,  $h_{SAR}$  depends only on difference between current position of satellite and shortest approach time so it is stationary. The ScanSAR pulse response depends on current satellite position and closest approach time rather than their difference. The ScanSAR azimuth spectrum is cyclostationary [20] and effective azimuth antenna weighting factor is shown in Fig. 1. Due to this time varying nature of ScanSAR system,

effective gain may vary periodically over azimuth causing scalloping in ScanSAR images. Similarly, effective range antenna weighting factor for a certain azimuth time varies as function of range position which results in ISB. A typical antenna weighting function with respect to range position is also shown in Fig. 1.

### 3. PROPOSED FRAMEWORK

#### 3.1. ScanSAR Imaging Model

Keeping in view (1) and (4), the single look complex (SLC) signal of ScanSAR in data domain can be modeled by following equation

$$S_c(r, x) = g(r, x)S_0(r, x) + o(r, x) \quad (5)$$

where  $S_0$  is ideal ScanSAR signal, which is free of scalloping and inter-Scan banding artifacts. In (5),  $g(r, x)$  and  $o(r, x)$  are two dimensional (2D) functions representing gain and intensity offset respectively. The gain function  $g(r, x)$  would represent two variations; variation of signal strength due to periodic changes of gain in azimuth direction that causes scalloping and gain variation of range antenna pattern (RAP) that would contribute towards inter-scan banding (ISB). Due to underlying independence between the phenomenons causing scalloping and ISB, 2D gain function can be split into two independent functions varying in azimuth and range directions. The offset function  $o(r, x)$  in (5) takes into account variations in noise floor, background scatter energy and atmospheric conditions. (5) can re-written as

$$\begin{aligned} S_c(r, x) &= g_X(x) [g_R(r)S_0(r, x) + o_R(r)] + o_X(x) \\ &= g_X(x)S_s(r, x) + o_X(x) \end{aligned} \quad (6)$$

where

$$S_s(r, x) = g_R(r)S_0(r, x) + o_R(r) \quad (7)$$

and

$$\begin{aligned} g(r, x) &= g_X(x)g_R(r) \\ o(r, x) &= o_X(x) + o_R(r)g_X(x) \end{aligned} \quad (8)$$

(6) to (8) are obtained by assuming that  $o(r, x)$  and  $g(r, x)$  can also be split into functions given by (8). The terms of (6) to (8) are explained as follows

- $S_c(r, x)$ : raw SLC signal from ScanSAR with inherent scalloping and inter-Scan banding.
- $S_0(r, c)$ : ideal image without any scalloping or ISB.
- $S_s(r, x)$ : ScanSAR signal corrupted with ISB only (no scalloping artifact).

- $g_X(x)$ : gain variation in azimuth direction.
- $g_R(r)$ : gain variation function in range direction.
- $o_X(x)$ : azimuth dependent offset contributing towards scalloping.
- $o_R(r)$ : range dependent offset contributing towards ISB.

We proposed a novel framework to remove scalloping and ISB using Kalman filters in azimuth and range direction sequentially. First of all we solve (6) to find  $S_s(r, x)$  using Kalman filter and then to solve (7) to find  $S_0(r, x)$ . The formulation of Kalman filters for solving (6) and (7) are given in Subsections 3.2 and 3.3 respectively.

### 3.2. Removal of Scalloping

Let  $\mathbf{S}_c$  be matrix representation of a ScanSAR signal  $\mathbf{S}_c$ .  $S_c(i, j)$  represents element of  $\mathbf{S}_c$  at  $i$ -th position in range direction and  $j$ -th location in azimuth direction, corresponding to SLC signal  $S_c(r, x)$ . Let  $\mathbf{S}_c$  be comprised of  $L$  total number of subswaths in a ScanSAR image. Let  $\mathbf{S}_c^{(l)}$  be  $l$ -th subswath in  $\mathbf{S}_c$ , i.e.,  $\mathbf{S}_c = [\mathbf{S}_c^{(1)}, \mathbf{S}_c^{(2)}, \dots, \mathbf{S}_c^{(L)}]^T$  (where  $T$  represents transpose).  $\mathbf{S}_c^{(l)}$  is an  $M \times N$  matrix with  $M$  and  $N$  are number of samples in range and azimuth directions respectively. The  $\mathbf{S}_c^{(l)}$  is comprised of  $N$  columns such that  $\mathbf{S}_c^{(l)} = [\mathbf{s}_c^{1(l)}, \mathbf{s}_c^{2(l)}, \dots, \mathbf{s}_c^{N(l)}]$  and  $\mathbf{s}_c^{j(l)} = [\mathbf{s}_{c_1}^{j(l)}, \mathbf{s}_{c_2}^{j(l)}, \dots, \mathbf{s}_{c_M}^{j(l)}]^T$ . The  $l$ -th subswath in ScanSAR signal can be given as

$$\mathbf{S}_c^l = \left[ \mathbf{s}_c^{1(l)}, \mathbf{s}_c^{2(l)}, \dots, \mathbf{s}_c^{N(l)} \right] = \begin{bmatrix} \mathbf{s}_{c_1}^{1(l)} & \mathbf{s}_{c_1}^{2(l)} & \dots & \mathbf{s}_{c_1}^{N(l)} \\ \mathbf{s}_{c_2}^{1(l)} & \mathbf{s}_{c_2}^{2(l)} & \dots & \mathbf{s}_{c_2}^{N(l)} \\ \vdots & \vdots & \ddots & \vdots \\ \mathbf{s}_{c_M}^{1(l)} & \mathbf{s}_{c_M}^{2(l)} & \dots & \mathbf{s}_{c_M}^{N(l)} \end{bmatrix} \quad (9)$$

Each column of  $\mathbf{S}_c^{(l)}$  comprises of  $M$  number of samples in range direction for a certain azimuth position  $j$  can be represented using (6)

$$\mathbf{s}_c^{j(l)} = g_X^{j(l)} \mathbf{s}_s^{j(l)} + o_X^{j(l)} + \mathbf{v}^{j(l)} \quad j \in 1, n \quad (10)$$

where  $g_X^{j(l)}$  is gain at  $j$ -th azimuth position in  $l$ -th subswath and  $o_X^{j(l)}$  is offset as a function of azimuth position for  $l$ -th subswath, and  $\mathbf{v}^{j(l)}$  is measurement noise. We assume that  $g_X^{j(l)}$  and  $o_X^{j(l)}$  varies as function of azimuth only and it remains constant for all samples in range direction for a certain azimuth location  $j$ , and subswath  $l$ . In order to remove scalloping, gain and offset parameters should be found from range samples for each azimuth location in the subswath. If we assume that ScanSAR scatters follow Gaussian distribution, then problem in (10)

can be looked as to find unknowns ( $g_x$  and  $o_X$ ) corrupted with Gaussian noise. In this scenario, Kalman filters [21] can be employed to estimate unknowns. Kalman filter is recursive, efficient, robust, easy to real-time implement filter and requires fewer number of observations for 'best' estimation of unknowns.

Kalman filter employs state space technique and iterative steps of prediction and correction. To solve 10, Kalman filter will be used to find minimum mean square error (MMSE) estimate of state vector  $\mathbf{z}^{j(l)} = [g_X^{j(l)}, o_X^{j(l)}]^T$  for each azimuth sampling position in the subswath. For sake of simple representation we can drop subscripts  $j$  and  $(l)$  from above notations. The problem at hand, is to find  $2 \times 1$  state vector  $\mathbf{z}$  from  $m \times 1$  observation vector. The state equation can be given by simple stochastic difference equation.

$$\mathbf{z}_{k+1} = \mathbf{A}_k \mathbf{z}_k + \mathbf{w}_k \quad (11)$$

where  $\mathbf{A}$  is state transition matrix and  $\mathbf{w}_k = [w_k^1, w_k^2]^T$  are noise sources associated with gain and offset respectively. The state transition matrix is given by

$$\mathbf{A}_k = \begin{bmatrix} \mu_k & 0 \\ 0 & \nu_k \end{bmatrix} \quad (12)$$

where  $\mu_k$  and  $\nu_k$  are parameters indicating inter-state drift of gain and offset respectively. In case of ScanSAR model, it can be assumed that gain and offset remain constant in range direction at certain azimuth position for a subswath. Therefore, the best estimation results are produced if  $\mu_k$  and  $\nu_k$  are set to unit magnitude in (12). The observation model for (10) can be given as

$$s_{c_k} = \mathbf{h}_k \mathbf{z}_k + v_k \quad (13)$$

where  $\mathbf{h}_k = [s_{s_k}, 1]$  is observation vector and  $v_k$  is observation noise. If we assume that range samples at all azimuth locations follow the same statistical characteristics,  $\mathbf{h}_k$  can be kept same for all azimuth locations.

Let  $\hat{\mathbf{z}}_k^- \in \mathfrak{R}^2$  and  $\hat{\mathbf{z}}_k^+ \in \mathfrak{R}^2$  be a priori and posteriori estimates of state vector for  $k$ -th step respectively.  $\hat{\mathbf{z}}_k^-$  is estimate of state given the knowledge of process prior to step  $k$  and  $\hat{\mathbf{z}}_k^+$  is estimate of state given measurement  $s_{c_k}$ . For  $k$ -th sample in range direction, MMSE estimate  $\hat{\mathbf{z}}_k$  can be considered as following conditional expectation

$$\hat{\mathbf{z}}_k = E[\mathbf{z}_k | s_{c_1}, s_{c_2}, \dots, s_{c_k}] \quad (14)$$

The posteriori estimate of state given by (14) can be given as a linear combination of an a priori estimate and a weighted difference

between an actual measurement and a measurement prediction as given below [21]

$$\hat{\mathbf{z}}_k = \hat{\mathbf{z}}_k^- + \mathbf{k}_k (s_{c_k} - \mathbf{h}_k \hat{\mathbf{z}}_k^-) \quad (15)$$

A priori predictor estimate,  $\hat{\mathbf{z}}_k^-$  can be iteratively computed by using

$$\hat{\mathbf{z}}_k^- = \mathbf{A}_{k-1} \hat{\mathbf{z}}_{k-1} + E[\mathbf{w}_{k-1}] \quad (16)$$

In (15),  $\mathbf{k}_k$  is a  $2 \times 1$  vector called Kalman gain or blending factor that minimizes a posteriori error covariance. The  $\mathbf{k}_k$  can be given as [21]

$$\mathbf{k}_k = \frac{\mathbf{P}_k^- \mathbf{h}_k^T}{\mathbf{h}_k \mathbf{P}_k^- \mathbf{h}_k^T + \sigma_v^2} \quad (17)$$

where  $\sigma_v^2$  is measurement error co-variance. The a priori estimate error covariance can be given as

$$\mathbf{P}_k^- = E \left[ (\mathbf{z}_k - \hat{\mathbf{z}}_k^-) (\mathbf{z}_k - \hat{\mathbf{z}}_k^-)^T \right] \quad (18)$$

where  $e_k^- \equiv \mathbf{z}_k - \hat{\mathbf{z}}_k^-$  is called a priori estimate error. The a priori  $\mathbf{P}_k^-$  estimate error covariance can be iteratively calculated as

$$\mathbf{P}_k^- = \mathbf{A}_{k-1} \mathbf{P}_{k-1} \mathbf{A}_{k-1}^T + \mathbf{Q} \quad (19)$$

where  $\mathbf{Q} = \sigma_w^2 \mathbf{I}_2$  ( $\mathbf{I}_2$  is a  $2 \times 2$  identity matrix) is process noise covariance. Similarly, a posteriori estimate error covariance can be given as

$$\mathbf{P}_k = E \left[ (\mathbf{z}_k - \hat{\mathbf{z}}_k) (\mathbf{z}_k - \hat{\mathbf{z}}_k)^T \right] \quad (20)$$

where  $e_k \equiv \mathbf{z}_k - \hat{\mathbf{z}}_k$  is called posteriori estimate error. It is updated by using relation

$$\mathbf{P}_k = (\mathbf{I}_2 - \mathbf{K}_k \mathbf{h}_k) \mathbf{P}_k^- \quad (21)$$

where  $\mathbf{I}_2$  is a  $2 \times 2$  identity matrix. In order to initialize the solution of (17), the values of  $\hat{\mathbf{z}}_0$  and  $\mathbf{P}_0$  are required. We initialize with  $\hat{\mathbf{z}}_0 = [0, 0]^T$  and  $\mathbf{P}_0 = \mathbf{I}_2$  (where  $\mathbf{I}_2$  is  $2 \times 2$  matrix). For  $j$ -th azimuth position in a subswath of  $\mathbf{S}_c$ ,  $\hat{\mathbf{z}}$  is estimated for all samples in range direction. The process is repeated for all azimuth locations in the subswath. An element of scalloping free ScanSAR signal matrix  $\hat{\mathbf{S}}_s$  for  $l$ -th subswath can be estimated as follows

$$\hat{S}_s(i, j)^{(l)} = \left( S_c(i, j)^{(l)} - o_X^{j(l)} \right) / g_X^{j(l)} \quad (22)$$

where  $g_X^{j(l)}$  and  $o_X^{j(l)}$  are gain and offset for  $j$ -th location in azimuth direction for  $l$ -th subswath estimated by using (17). The scalloping is removed by using (22) for all subswaths in order to obtain  $\hat{\mathbf{S}}_s$ .

### 3.3. Removal of Inter-scan Banding

Let  $\hat{\mathbf{S}}_s$  be an  $M \times N$  matrix that represents descalloped SAR image obtained by applying (24). Let  $\hat{s}_s^i$  be  $i$ -th row of descalloped ScanSAR image  $\hat{\mathbf{S}}_s$ . The matrix representation of descalloped ScanSAR image can be written as

$$\hat{\mathbf{S}}_s = \begin{bmatrix} \hat{s}_s^1 \\ \hat{s}_s^2 \\ \vdots \\ \hat{s}_s^M \end{bmatrix} = \begin{bmatrix} \hat{s}_{s_1}^1 & \hat{s}_{s_2}^1 & \cdots & \hat{s}_{s_N}^1 \\ \hat{s}_{s_1}^2 & \hat{s}_{s_2}^2 & \cdots & \hat{s}_{s_N}^2 \\ \vdots & \vdots & \ddots & \vdots \\ \hat{s}_{s_1}^M & \hat{s}_{s_2}^M & \cdots & \hat{s}_{s_N}^M \end{bmatrix} \quad (23)$$

Using (7), descalloped SAR image can be written as

$$\hat{S}_s(i, j) = g_R(i)S_0(i, j) + o_R(j); \quad i \in [1, M] \text{ and } j \in [1, N] \quad (24)$$

Our aim is to find  $\mathbf{S}_0$  which is ideal ScanSAR image, free of both scalloping inter-scan banding. A row of  $\hat{\mathbf{S}}_s$  comprising of  $N$  number of samples in azimuth direction for  $i$ -th range position can be represented using (24)

$$\hat{s}_s^i = g_R^i s_0^i + o_R^i + \mathbf{v}_R^i \quad i \in 1, M \quad (25)$$

where  $g_R^i$  and  $o_R^i$  are gain and offset at  $i$  range position and  $\mathbf{v}_R^i$  is measurement noise. For sake of simplicity, we assume that  $g_R^i$  and  $o_R^i$  vary as function of range only and we are aiming to find MMSE estimate of state vector  $\mathbf{b}^i = [g_R^i, o_R^i]^T$  for each range sampling position in the subswath. Following the procedure given in Section 3.2, the state equation for range parameters can be given as

$$\mathbf{b}_{k+1} = \mathbf{A}_k^R \mathbf{b}_k + \mathbf{w}_k^R \quad (26)$$

where  $\mathbf{A}_k^R$  can be defined by using (12) but values of  $\mu_k$  and  $\nu_k$  may be different from the values used in case of scalloping and  $\mathbf{w}_k^R$  is process noise. Similarly, the observation model for (25) can be given as

$$\hat{s}_{s_k} = \mathbf{h}_k^R \mathbf{b}_k + v_k^R \quad (27)$$

where  $\mathbf{h}_k^R = [s_{0_k}, 1]$  is observation model in range direction and  $v_k^R$  is observation noise in range direction. A posteriori state estimate of  $\hat{\mathbf{b}}_k$  can be found as follows [21]

$$\hat{\mathbf{b}}_k = \hat{\mathbf{b}}_k^- + \mathbf{k}_k^R \left( S_{s_k} - \mathbf{h}_k^R \hat{\mathbf{b}}_k^- \right) \quad (28)$$

where  $\hat{\mathbf{b}}_k^- \approx E [\mathbf{b}_k | s_{s_1}, s_{s_2}, \dots, s_{s_{k-1}}]$  is called predictor estimate and vector  $\mathbf{k}_k^R$  is Kalman gain that minimizes a posteriori error covariance.

The  $\mathbf{k}_k^R$  can be given as [21]

$$\mathbf{k}_k^R = \frac{\mathbf{P}_k^- (\mathbf{h}_k^R)^T}{\mathbf{h}_k^R \mathbf{P}_k^- (\mathbf{h}_k^R)^T + (\sigma_v^R)^2} \tag{29}$$

where  $(\sigma_v^R)^2$  is measurement error co-variance in range direction. The a priori and a posteriori estimate error covariances,  $\mathbf{P}_k^-$  and  $\mathbf{P}_k$  can be calculated by using (19) and (20). For  $i$ -th range position of  $\mathbf{S}_s$ ,  $\hat{\mathbf{b}}$  is estimated for all samples in azimuth direction. The process is repeated for all range locations in  $\mathbf{S}_s$ . An element of scalloping free ScanSAR signal matrix  $\hat{\mathbf{S}}_0$  can be estimated as follows

$$\hat{S}_0(i, j) = (S_s(i, j) - o_R^i) / g_R^i; \tag{30}$$

where  $g_R^i$  and  $o_R^i$  are gain and offset for  $i$ -th location in range direction estimated by using (28).

#### 4. IMPLEMENTATION AND EXPERIMENTAL RESULTS

A number of experiments have been carried out on simulated as well as real ScanSAR images to remove scalloping and ISB artifacts. The simulated ScanSAR images are generated by introducing scalloping and banding artifacts in processed SAR images. As original SAR images are accessible, the performance of proposed technique can be quantified with simulated images. The proposed scheme was also tested on real ScanSAR image having residual scalloping artifacts. The initial conditions for estimation of gain and offset for azimuth and range positions are;  $\hat{\mathbf{z}}_0 = \hat{\mathbf{b}}_0 = [0, 0]^T$ ,  $\mathbf{P}_0 = \mathbf{I}_2$  and  $\mathbf{Q}_0 = 1 \times 10^{-5} \mathbf{I}_2$  (where  $\mathbf{I}_2$  is  $2 \times 2$  identity matrix).

##### 4.1. Simulation of Scalloping and ISB Artifacts

###### 4.1.1. Scalloping

Scalloping is a periodic noise as explained in Section 2. As explained in Section 2, system response is not parabolic rather it is parabolic in shape as shown in Fig. 1, which can be modeled by expression

$$\eta(r, x) = a|\sin(bx + \vartheta)| + \zeta_r + \zeta_x \tag{31}$$

where ‘ $a$ ’ is constant representing the average peak value of scalloping artifact; ‘ $b$ ’ is constant which varies with respect to burst time;  $\vartheta$  is a random variable representing the phase variation of scalloping artifact;  $\zeta_r$  and  $\zeta_x$  are random variables representing the intensity variation due

to measurement noise in range and azimuth directions respectively. The expression given in above equation produces scalloping artifacts close to artifacts found in real ScanSAR systems.

#### 4.1.2. Inter-scan Banding

ISB is possibly due to temporal change of the RAP and the variation in the noise floor and the background intensities [15]. In order to simulate ISB artifact, we used a polynomial representing an arc to represent inter-subswath variation of RAP and produced random shifts in inter-subswath intensity. The polynomial to represent the arc is estimated based on the ISB artifacts in ScanSAR images given in [18].

## 4.2. Experimental Results

A processed SAR image shown in Fig. 2(a) was corrupted with scalloping artifact having inter-swath phase and intensity variations as shown in Fig. 2(b). The proposed descloping technique was employed to remove the scalloping from corrupted image. The ScanSAR image after removal of scalloping is shown in Fig. 2(c). It is observed that proposed technique can remove scalloping and produce an image with visual quality close to original image. It is worth mentioning that the proposed technique would not alter the radiometric calibration of

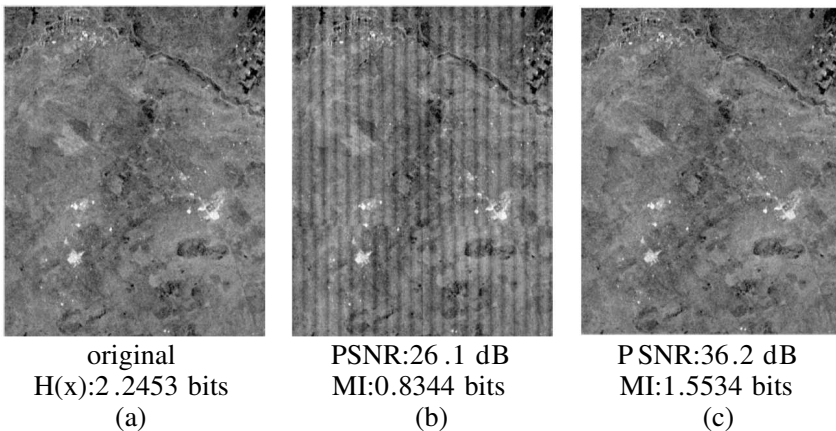


**Figure 2.** Scalloping removal using proposed technique; (a) original processed SAR image; (b) SAR image corrupted with scalloping pattern in subswaths with variable phase and intensity; (c) descalloping by employing proposed technique.

ScanSAR images as proposed Kalman filter is unbiased filter. The proposed scalloping and ISB removal technique preserve the average radiometric value of ScanSAR image as evident in Fig. 2.

In case of simulated ScanSAR images, original images (free of scalloping artifacts) are available, so performance of proposed descalloping technique can be quantified. Two performance measuring metrics, i.e., peak signal-to-noise ratio (PSNR) and mutual information (MI) are employed to quantify the image enhancement obtained using proposed technique. Let  $\mathbf{S}_0$  and  $\mathbf{S}_c$  be original SAR image and SAR image corrupted with scalloping artifact respectively. If  $\hat{\mathbf{S}}_0$  is descalloped ScanSAR image, the PSNR is given as

$$\text{PSNR} = 10 \log \left[ \frac{DR^2}{\frac{1}{M \times N} \sum_i \sum_j e^2(i, j)} \right] \quad (32)$$

where  $M$  and  $N$  are range and azimuth samples in SAR image,  $e^2(i, j)$  is error function between  $\mathbf{S}_0$  and  $\hat{\mathbf{S}}_0$  in  $i$ -th range position and  $j$ -th azimuth positions and  $DR = \max(\mathbf{S}_0) - \min(\mathbf{S}_0)$ . The mutual information between original image,  $\mathbf{S}_0$  and corrected image,  $\hat{\mathbf{S}}_0$  is defined as

$$MI(\mathbf{S}_0; \hat{\mathbf{S}}_0) = \sum_{s_0, \hat{s}_0} P(s_0, \hat{s}_0) \log \frac{P(s_0, \hat{s}_0)}{P(s_0)P(\hat{s}_0)} \quad (33)$$

where  $P(s_0, \hat{s}_0)$  is joint probability mass function, and  $P(s_0)$  and  $P(\hat{s}_0)$  are marginal probability mass functions. The proposed descalloping scheme improved PSNR value from 26.2 dB to 36.1 dB and increased mutual MI from 0.8344 bits to 1.5534 bits for Fig. 2.

Another way to highlight the effectiveness of descalloping technique could be to observe intensity as a function of azimuth position in ScanSAR image. The azimuth intensity profiles extracted from the part of first subswath of simulated ScanSAR image (Fig. 2(b)) is shown in Fig. 3(a). The periodic variations in the intensity due to scalloping are quite visible in the intensity profile. The intensity azimuth profiles extracted from the same part of first subswath of the descalloped image (Fig. 2(c)) is shown in Fig. 3(b). The significant reduction in periodic variation in intensity profile in azimuth can be observed in Fig. 3(b) and restored signal is close to original image. The error in intensity of descalloped image compared to original image is shown in Fig. 3(c). The comparison of intensity error of restored simulated ScanSAR image and intensity error of simulated SAR image exhibits the capability of proposed descalloping technique.

In order to test proposed scheme for removal of inter-Scan banding (ISB) in ScanSAR image, a typical inter-scan banding artifacts is

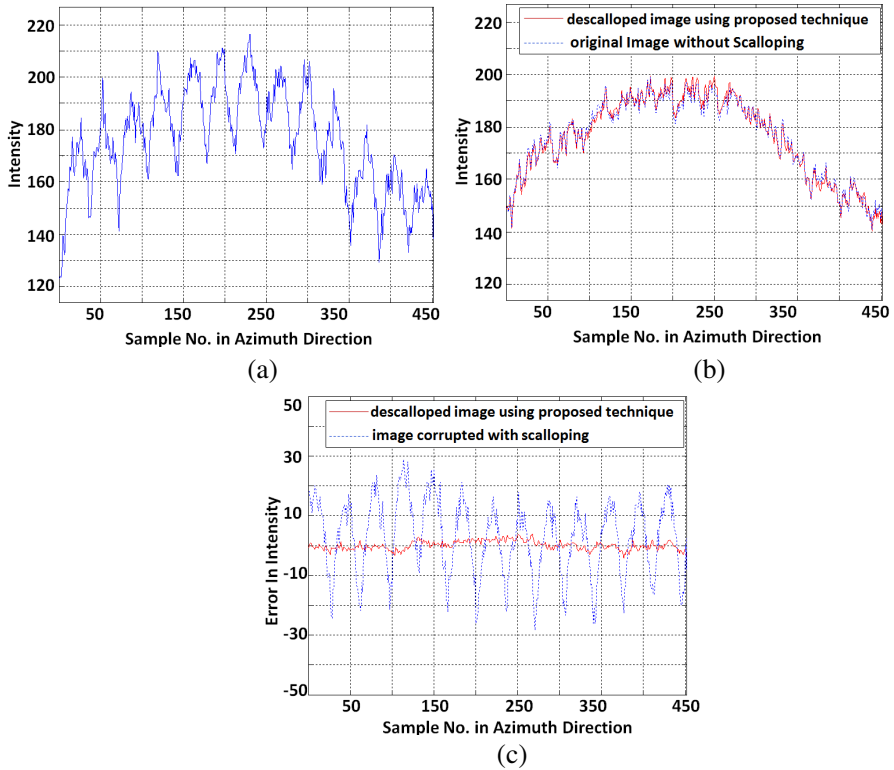


**Figure 3.** Comparison of azimuth intensity profiles; (a) azimuth intensity profile extracted from a part of first subswath of SAR image corrupted with scalloping (Fig. 2(b)); (b) azimuth intensity profile extracted from the same part of first subswath of SAR image descalloped using proposed technique (Fig. 2(c)); (c) azimuth intensity error of descalloped image. Note: The intensity is normalized to 255, the gray level range used to display images.

overlaid on processed SAR image and this corrupted SAR image is used as test image for proposed ISB removal technique. The simulated ISB test image is shown in Fig. 4(a). The initial conditions to estimate gain and offset in range direction by using (28) are same as were used for removal of scalloping. Once gain and offset for all range positions are known, image is corrected by applying (30). The image corrected by applying proposed technique is shown in Fig. 4(b). It can be observed that proposed technique has considerably reduced the inter-Scan banding artifact. The proposed ISB removal scheme improved PSNR value from 33.6 dB to 42.1 dB and increased MI from 1.6132 bits to 2.1757 bits.

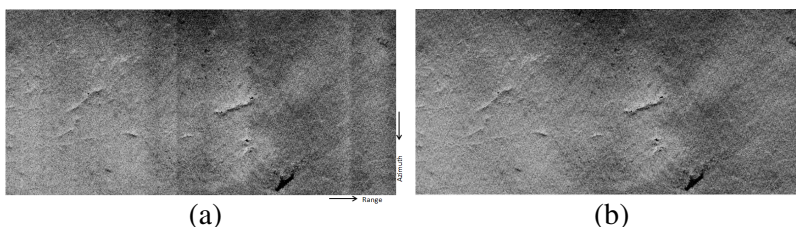


**Figure 4.** Removal of inter-scan banding; (a) ScanSAR image with inherent inter-scan banding (PSNR: 34 : 2 dB, MI: 1 : 6132 bits); (b) ScanSAR image after removal of inter-scan banding by employing proposed technique (PSNR: 42 : 1 dB, MI: 2 : 1757 bits).

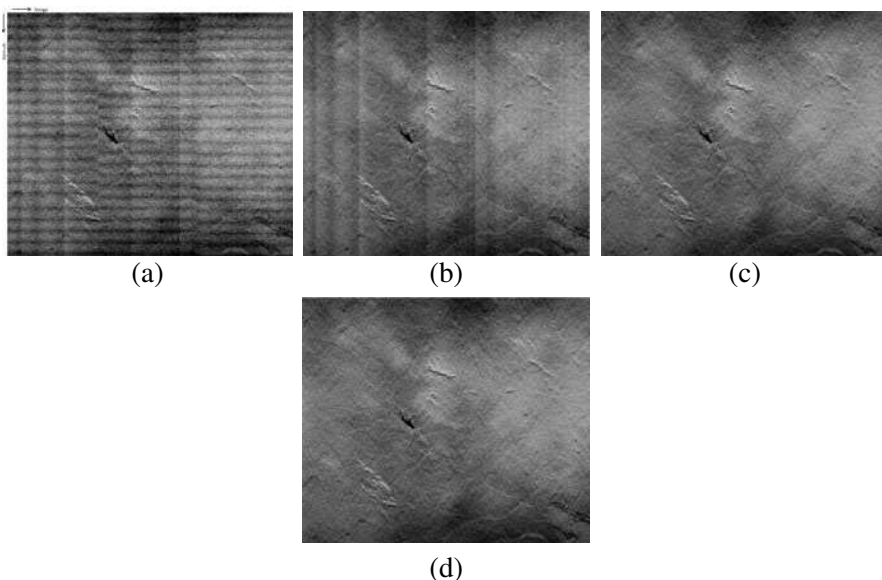


**Figure 5.** Removal of scalloping and inter-scan banding; (a) SAR image corrupted with inter-scan banding and scalloping artifacts (PSNR: 25 : 3 dB, MI: 1 : 0465 bits); (b) image after removal of scalloping using proposed technique, the inter-scan banding is still visible (PSNR: 33 : 6 dB, MI: 1 : 5634 bits); (c) ScanSAR image after removal of inter-scan banding from image shown in (b) (PSNR: 35 : 9 dB, MI: 1 : 7818 bits); (d) ScanSAR image by first removing ISB and then removing scalloping (PSNR: 35 : 8 dB, MI: 1 : 7813 bits).

The proposed descloping and ISB removal technique was applied to test image corrupted with both scalloping and ISB artifacts. The test images is created by adding scalloping and ISB artifacts

sequentially and resulting test image is shown in Fig. 5(a). The proposed technique was first used to remove scalloping by applying Kalman filters on all positions in azimuth direction and descalloped image by following the same initial conditions used to produce results shown in Fig. 2. The descalloped image is shown in Fig. 5(b). It can be seen that scalloping has been removed but inter-scan banding artifact is present. In order to remove inter-scan banding, the Kalman filter given in Section 3.3 was applied on all range positions in the ScanSAR image and final image is shown in Fig. 5(c). Results shown in Fig. 2 to Fig. 5 support that the proposed technique can be directly employed as an effective procedure for removing scalloping and inter-scan banding

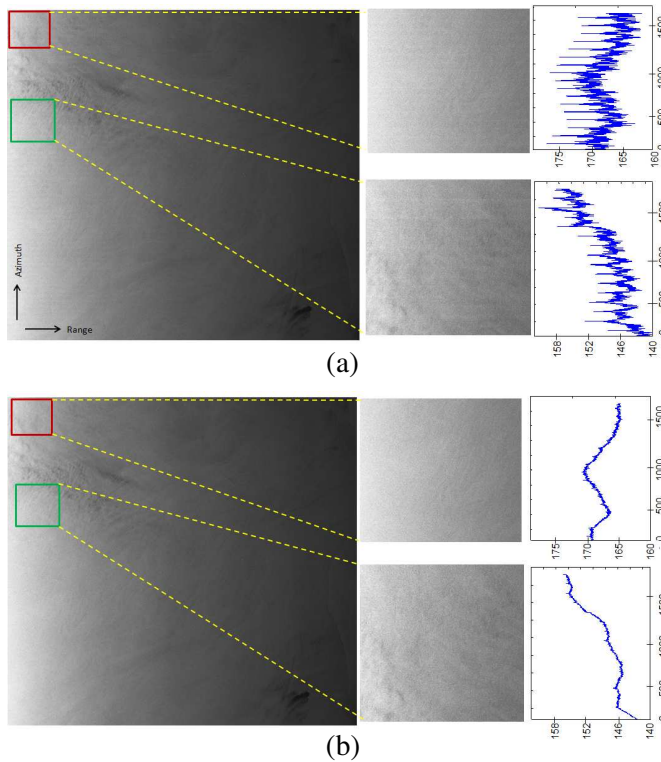


**Figure 6.** Removal of scalloping from real ScanSAR image; (a) real ALOS/PALSAR ScanSAR image after scalloping-calibration but residual scalloping artifacts can be seen in zoomed patches; (b) image after removal of scalloping using proposed technique. The azimuth intensity profiles of zoomed patches in original and processed images are shown with their respective patches.

in ScanSAR image formation processing. The proposed technique is invariant to order of removal of scalloping and ISB. Fig. 5(d) shows ScanSAR image, where ISB removal was performed prior to removal of scalloping. It can be observed that reversal of removal order of scalloping and ISB does not have effect on results. This supports our initial assumption of decoupling scalloping and ISB.

Finally, the proposed technique is applied to real ALOS/PALSAR ScanSAR image in ocean area as shown in Fig. 6(a). The ScanSAR image shown in Fig. 6(a) has been obtained after accurate Doppler centroid estimation in image formation processing and employing dynamic filtering [15], but still residual scalloping artifacts can be observed. The ScanSAR image obtained after applying proposed technique is shown in Fig. 6(b). The selected patches from the original and processed images are enlarged along with intensity variations in azimuth positions in the respective parts of Fig. 6. The comparison of visual quality and azimuth intensity profiles exhibits that the proposed technique can also be applied as post-processing step for removal of residual scalloping in scalloping-calibrated ScanSAR images to enhance their quality.

## 5. CONCLUSION

A novel scheme is proposed to remove scalloping and inter-scan banding (ISB) in ScanSAR images. The scalloping and ISB are modeled by parameters varying in azimuth and range directions respectively, and these parameters are estimated by using minimum mean square error Kalman filters. For estimation of scalloping parameters in a subswath, range samples for each azimuth position are taken as observations to obtain recursive MMSE estimate. Similarly, for range parameters, azimuth samples for each range position are taken as observations to obtain recursive MMSE estimate. The estimated parameters are used to remove scalloping and ISB artifacts sequentially. The simulation results exhibit potential of proposed technique to remove scalloping and ISB in ScanSAR imaging. The The proposed technique is robust, and does not require knowledge about SAR antenna pattern or system calibration parameters.

## ACKNOWLEDGMENT

The work described in the paper was supported in part by the National Key Basic Research Program Project under Grant 2010CB731902, and in part by the National Natural Science Foundation of China under Grant No. 61132006.

## REFERENCES

1. An, D. X., Z.-M. Zhou, X.-T. Huang, and T. Jin, "A novel imaging approach for high resolution squinted spotlight SAR based on the deramping-based technique and azimuth nlcs principle," *Progress In Electromagnetics Research*, Vol. 123, 485–508, 2012.
2. Chen, J., J. Gao, Y. Zhu, W. Yang, and P. Wang, "A novel image formation algorithm for high-resolution wide-swath spaceborne SAR using compressed sensing on azimuth displacement phase center antenna," *Progress In Electromagnetics Research*, Vol. 125, 527–543, 2012.
3. Koo, V. C., Y. K. Chan, V. Gobi, M. Y. Chua, C. H. Lim, C.-S. Lim, C. C. Thum, T. S. Lim, Z. bin Ahmad, K. A. Mahmood, M. H. Bin Shahid, C. Y. Ang, W. Q. Tan, P. N. Tan, K. S. Yee, W. G. Cheaw, H. S. Boey, A. L. Choo, and B. C. Sew, "A new unmanned aerial vehicle synthetic aperture radar for environmental monitoring," *Progress In Electromagnetics Research*, Vol. 122, 245–268, 2012.
4. Zhu, D.-Y., B. Tian, and Z.-D. Zhu, "A novel moving target detection approach for dual-channel SAR system," *Progress In Electromagnetics Research*, Vol. 115, 191–206, 2011.
5. Ismail, A., M. Mohammadpoor, R. S. A. Raja Abdullah, and A. F. Abas, "A circular synthetic aperture radar for on-the-ground object detection," *Progress In Electromagnetics Research*, Vol. 122, 269–292, 2012.
6. Park, J.-I. and K.-T. Kim, "A comparative study on isar imaging algorithms for radar target identification," *Progress In Electromagnetics Research*, Vol. 108, 155–175, 2010.
7. Martinez-Lorenzo, J. A., F. Quivira, and C. M. Rappaport, "SAR imaging of suicide bombers wearing concealed explosive threats," *Progress In Electromagnetics Research*, Vol. 125, 255–172, 2012.
8. Ren, S., W. Chang, T. Jin, and Z. Wang, "Automated SAR reference image preparation for navigation," *Progress In Electromagnetics Research*, Vol. 121, 535–555, 2011.
9. Chiang, C.-Y., Y.-L. Chang, and K.-S. Chen, "SAR image simulation with application to target recognition," *Progress In Electromagnetics Research*, Vol. 119, 35–57, 2011.
10. Meta, A., P. Prats, U. Steinbrecher, J. Mittermayer, and R. Scheiber, "Terrasar-x topsar and scansar comparison," *2008 7th European Conference on Synthetic Aperture Radar (EUSAR)*, 1–4, Jun. 2008.
11. Bamler, R., "Optimum look weighting for burst-mode and

- ScanSAR processing,” *IEEE Transactions on Geoscience and Remote Sensing*, Vol. 33, No. 3, 722–725, May 1995.
12. Vigneron, C. M., “Radiometric image quality improvement of ScanSAR data,” M.S. Thesis, Carleton University, Ottawa, ON, Canada, 2001.
  13. Shimada, M., “Long-term stability of L-band normalized radar cross section of Amazon rainforest using the JERS-1 SAR,” *Canadian J. of Remote Sensing*, Vol. 31, No. 1, 132–137, 2005.
  14. Shimada, M., O. Isoguchi, T. Tadono, and K. Isono, “Palsar radiometric and geometric calibration,” *IEEE Transactions on Geoscience and Remote Sensing*, Vol. 47, No. 12, 3915–3932, Dec. 2009.
  15. Shimada, M., “A new method for correcting ScanSAR scalloping using forests and inter-scan banding employing dynamic filtering,” *IEEE Transactions on Geoscience and Remote Sensing*, Vol. 47, No. 12, 3933–3942, Dec. 2009.
  16. Romeiser, R., J. Horstmann, and H. Graber, “A new scalloping filter algorithm for ScanSAR images,” *2010 IEEE International Geoscience and Remote Sensing Symposium, IGARSS’10*, 4079–4082, Jul. 2010.
  17. Feng, M. and H. Jun, “The critical techniques for ScanSAR radiometric correction,” *1st Asian and Pacific Conference on Synthetic Aperture Radar, APSAR 2007*, 10–13, Nov. 2007.
  18. Bast, D. C. and I. G. Cumming, “Radarsat ScanSAR roll angle estimation,” *2002 IEEE International Geoscience and Remote Sensing Symposium, IGARSS’02*, Vol. 1, 152–154, 2002.
  19. Iqbal, M. and J. Chen, “Removal of scalloping in ScanSAR images using kalman filters,” *2012 IEEE International Geoscience and Remote Sensing Symposium, IGARSS’12*, 260–263, Jul. 2012.
  20. Guarnieri, A. M. and C. Prati, “ScanSAR focusing and interferometry,” *IEEE Transactions on Geoscience and Remote Sensing*, Vol. 34, No. 4, 1029–1038, Jul. 1996.
  21. Brown, R. G. and P. Y. C. Hwang, *Introduction to Random Signals and Applied Kalman Filtering*, John Wiley and Sons, Inc., 1992.